J. Fluid Mech. (1978), *vol.* 84, *part* 2, *pp.* 337–358
Printed in Great Britain

The Korteweg–de Vries equation and water waves. Part 3. Oscillatory waves

By JOSEPH L. HAMMACK

Coastal and Oceanographic Engineering Laboratory, Department of Engineering Sciences, University of Florida, Gainesville

AND HARVEY SEGUR

Department of Mathematics, Clarkson College of Technology, Potsdam, New York†

(Received 2 February 1977 and in revised form 18 April 1977)

Water-wave experiments are presented showing the evolution of finite amplitude waves in relatively shallow water when *no solitons* are present. In each case, the initial wave is rectangular in shape and wholly below the still water level; the amplitude of the wave is varied. The asymptotic solution of the Korteweg–de Vries (KdV) equation in the absence of solitons (Ablowitz & Segur 1976) is compared with observed evolution. In addition, the asymptotic solution of the linearized KdV equation (a linear dispersive model) is compared with both the KdV solution and experiments. This comparison is a natural consequence of the fact that, in the absence of solitons, the asymptotic solutions of the KdV equation and its linearized version are qualitatively similar. Both the experiments and the model equations suggest that the asymptotic wave structure consists of a negative triangular wave, travelling with a speed $(gh)^{\frac{1}{2}}$, followed by a train of modulated oscillatory waves which travel more slowly. Quantitative comparisons are made for the amplitude, shape and decay rate of the leading wave and the amplitude, dominant wavenumbers and velocities of the trailing wave groups. Over the parameter range of the experiments, asymptotic KdV theory predicts more closely the observed behaviour. The leading wave is observed to decay more rapidly than the trailing wave groups; hence the leading wave becomes less prominent with time. This is in agreement with the KdV solution, whereas just the opposite is predicted by linear theory. Linear predictions for the trailing wave groups are accurate only when they agree with the KdV predictions. Both models predict the evolution of short waves in the trailing wave region. When the short waves are unstable ($k > 1{\cdot}36$), either group disintegration or focusing into envelope solitons is possible. Both of these phenomena are observed in the experiments; neither is predicted by long-wave models. The nonlinear Schrödinger equation is reviewed and tested as a model of these unstable wave groups. There is some evidence that the KdV equation and the nonlinear Schrödinger equation can be patched together to provide an asymptotic description of these unstable groups.

---

† Present address: Aeronautical Research Associates of Princeton, Inc., Princeton, New Jersey.

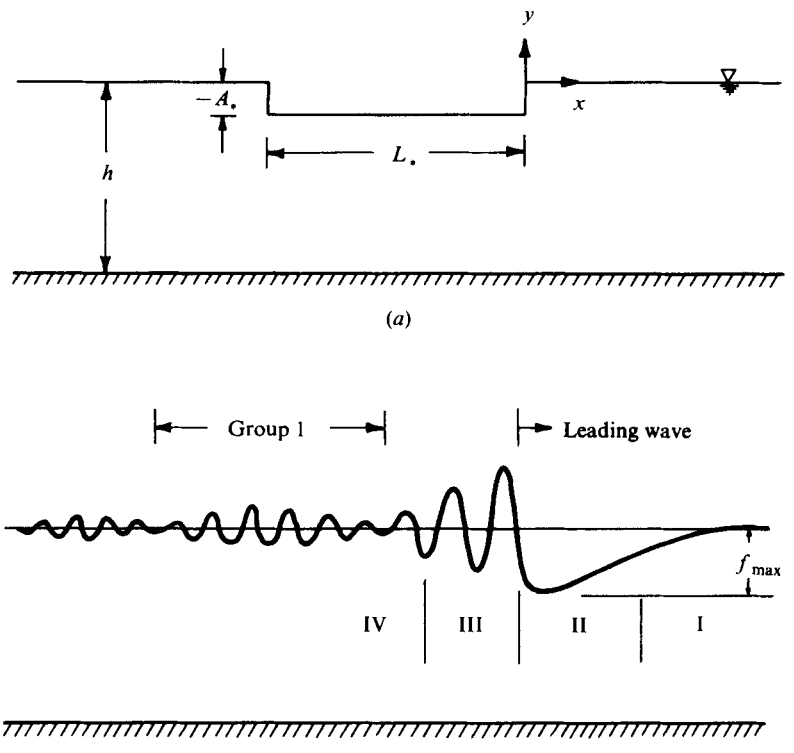

FIGURE 1. (*a*) Rectangular initial ($\tau = 0$) wave. (*b*) Asymptotic ($\tau \to \infty$) structure of initial waves when no solitons evolve: I, $\chi = O(\tau)$; II, $|\chi| \leqslant O(\tau^{\frac{1}{3}})$; III, $-\chi = O[\tau^{\frac{1}{3}}(\ln\tau)^{\frac{2}{3}}]$; IV, $-\chi = O(\tau)$.

1. Introduction

This paper is the third in a series on the propagation of finite amplitude water waves in relatively shallow water. Previous papers focused on the solution of the Korteweg–de Vries (KdV) equation for modelling the evolution of shallow-water waves (part 1; Segur 1973) and on the accuracy of this model in predicting the observed evolution of such waves in laboratory experiments (part 2; Hammack & Segur 1974). The outstanding feature of the KdV model is the important role played by solitons. Previous experiments were chosen to emphasize the role of solitons in the evolution of long water waves.

It is also easy to generate experimentally long initial waves which produce no solitons; hence all of the energy in the initial data eventually is found in an oscillatory wave train. For these waves, the accuracy of the KdV model must be tested again. Moreover, the predictions of a linear long-wave model (e.g. Jeffreys & Jeffreys 1972, pp. 512–517) are qualitatively similar to those of the KdV model for these waves; hence the necessity of the nonlinear KdV equation for these waves is also in question.

The objective of this paper is to resolve the above questions experimentally. In each experiment, the initial wave is rectangular in shape and wholly below the still water level, as shown in figure 1 (*a*). The wave train which travels to the right (or left) evolves into a form similar to that in figure 1 (*b*), with no solitons. The observed evolu-

tion of these waves is compared with the behaviour predicted by the KdV model (Ablowitz & Segur 1976) and with that predicted by a linear long-wave model (Jeffreys & Jeffreys 1972).

There are two major limitations to such a comparison. First, neither model accounts for viscous effects, and no attempt has been made here to correct this deficiency. Consequently, some features of the predicted solutions cannot be tested conclusively. Second, long initial waves generate short waves whose behaviour is poorly predicted by either long-wave model. In §4 we discuss how to patch the KdV model to a short-wave model (the nonlinear Schrödinger equation) in order to predict the behaviour of these waves.

The organization of this paper is as follows. The relevant consequences of the models in question (the KdV, linear dispersive and nonlinear Schrödinger equations) are reviewed in §2. A brief description of the experiments is given in §3, followed by a discussion of the wave evolution observed in these experiments. Detailed comparisons of various aspects of the theory and experiments are found in §4, followed by our major conclusions in §5.

2. Review of the theories

2.1. *The KdV equation*

The derivation of the KdV equation for two-dimensional surface waves propagating in only one direction in relatively shallow water was discussed in part 2. For a wave of amplitude $\eta(x,t)$ propagating to the right in a channel of uniform depth h, the dimensional KdV equation is

$$\eta_t + (gh)^{\frac{1}{2}}\eta_x + \tfrac{3}{2}(gh)^{\frac{1}{2}}h^{-1}\eta\eta_x + \tfrac{1}{6}h^2(gh)^{\frac{1}{2}}\eta_{xxx} = 0. \tag{1}$$

In terms of non-dimensional variables

$$\chi = h^{-1}[x-(gh)^{\frac{1}{2}}t], \quad \tau = \tfrac{1}{6}(g/h)^{\frac{1}{2}}t, \quad f(\chi,\tau) = \tfrac{3}{2}h^{-1}\eta(x,t), \tag{2}$$

this becomes

$$f_\tau + 6ff_\chi + f_{\chi\chi\chi} = 0. \tag{3}$$

For the experiments considered herein, the initial data for (3) consisted of negative rectangular waves (as shown in figure 1*a*):

$$f(\chi,0) = \left\{\begin{array}{lll} 0 & \text{for} & \chi > 0, \\ -A & \text{for} & -L < \chi < 0, \\ 0 & \text{for} & \chi < -L, \end{array}\right\} \tag{4}$$

where $A = 3A_*/2h$ and $L = L_*/h$. No solitons can arise from these negative waves (cf. part 1) and the linear eigenvalue problem becomes

$$\psi_{\chi\chi} + [k^2 + f(\chi,0)]\psi = 0, \tag{5}$$

subject to the boundary conditions (for real k)

$$\psi \sim \begin{cases} e^{-ik\chi} + r(k)\,e^{ik\chi}, & \chi \to +\infty, \\ (a(k))^{-1}e^{-ik\chi}, & \chi \to -\infty. \end{cases} \tag{6}$$

Here k is a dimensionless wavenumber and $r(k)$, the reflexion coefficient for the potential $f(\chi,0)$, can be interpreted as a 'nonlinear Fourier transform' (Ablowitz

et al. 1974). For negative rectangular waves, $r(\frac{1}{2}k)$ can be found explicitly (cf. Schiff 1968, p. 103):

$$r(\tfrac{1}{2}k) = \frac{A\sin\{(\frac{1}{4}k^2-A)^{\frac{1}{2}}L\}}{(\frac{1}{2}k^2-A)\sin\{(\frac{1}{4}k^2-A)^{\frac{1}{2}}L\}+\frac{1}{2}ik(\frac{1}{4}k^2-A)^{\frac{1}{2}}\cos\{(\frac{1}{4}k^2-A)^{\frac{1}{2}}L\}}. \tag{7}$$

The asymptotic (large τ) solution of (3) when no solitons exist is presented by Ablowitz & Segur (1976) and we state here their major results. For the initial data of interest herein, $r(0) = -1$ and the solution is developed in four separate regions which are connected by matching zones (see figure 1*b*). In region I, where $\chi = O(\tau)$, corresponding to the upstream portion of the advancing wave front, the wave amplitude is exponentially small. In region II, where $|\chi| \leqslant O(\tau^{\frac{1}{3}})$ and which will be termed the leading wave, the asymptotic solution is self-similar and approaches the exact solution

$$f(\chi,\tau) = (3\tau)^{-\frac{2}{3}}(\tfrac{1}{2}\tilde{\zeta}) \tag{8}$$

for $\chi < 0$, where

$$\tilde{\zeta} = \chi/(3\tau)^{\frac{1}{3}} \tag{9}$$

is the similarity variable. As $\tilde{\zeta}\to-\infty$, the expansion in region II breaks down according to

$$\begin{aligned} f(\chi,\tau) \sim (3\tau)^{-\frac{2}{3}}(-2\zeta)\{-\tfrac{1}{4}-\tfrac{1}{2}(-2\zeta)^{-\frac{3}{2}}+\ldots \\ +[(3\tau)^{-\frac{2}{3}}\kappa M(-2\zeta)^{-\frac{5}{4}}\exp(\tfrac{1}{3}(-2\zeta)^{\frac{3}{2}})+\ldots]+\ldots\}, \end{aligned} \tag{10}$$

where

$$\zeta = (\chi+\chi_0)/(3\tau)^{\frac{1}{3}} \tag{11}$$

represents an 'asymptotically preferred' co-ordinate which is obtained from the original one by a translation

$$\chi_0 = -ir'(0)/2r(0) = \tfrac{1}{2}ir'(0). \tag{12}$$

The parameter M in (10) is determined from the initial data by

$$M = \{r''(0)r(0)-[r'(0)]^2\}/8r(0) = \tfrac{1}{8}\{r''(0)+[r'(0)]^2\} \tag{13}$$

and κ is a constant of integration ($\kappa \approx 0{\cdot}8$). From (7) it follows that

$$\chi_0 = 1/A^{\frac{1}{2}}\tanh A^{\frac{1}{2}}L, \quad M = 1/2A\sinh^2 A^{\frac{1}{2}}L \tag{14}$$

for initial data given by (4).

The location of the amplitude extremum in region II, where $df/d\zeta = 0$ and $\zeta \approx \zeta_0$, is found from (10); this extremum occurs where

$$\tfrac{1}{2}(-2\zeta_0)^{\frac{3}{2}} \sim \ln 3\tau - \tfrac{3}{8}\ln(-2\zeta_0) - \tfrac{3}{2}\ln(2\kappa M). \tag{15}$$

For very large times the effect of the initial data contained in the parameter M is lost, and (15) can be approximated by

$$(-2\zeta_0) \sim (2\ln 3\tau)^{\frac{2}{3}}. \tag{16}$$

For the experiments to be presented the maximum time over which the wave properties are measured is $3\tau = 100$ and the effects of the initial data cannot be neglected. The maximum amplitude $f_{\max}$ of the wave front is given by

$$f_{\max} \sim -\tfrac{1}{4}(3\tau)^{-\frac{2}{3}}(-2\zeta_0). \tag{17}$$

For very large times (16) and (17) together indicate that the amplitude of the wave front decays as $[2\ln(3\tau)/3\tau]^{\frac{2}{3}}$.

The breakdown of (10) in region II as $\zeta \to -\infty$ requires the existence of region III (see figure 1*b*), where the solution behaves like a 'dissipationless shock layer'. Here the character of the solution must change from monotonic in region II to oscillatory in region IV. (Details of the shock layer will not be presented or compared with experiment.) In region IV, where $-\chi = O(\tau)$, the asymptotic solution is given by

$$f(\chi,\tau) \sim (3\tau)^{-\frac{1}{2}} 2dk^{\frac{1}{2}} \cos\theta - (3\tau)^{-1}k^{-1}\{2d^2 - 2d^2\cos 2\theta\}, \tag{18}$$

where

$$d^2 = (4\pi)^{-1}\ln\left[1 - |r(\tfrac{1}{2}k)|^2\right], \tag{19}$$

$$\theta \sim (3\tau)\{\tfrac{2}{3}k^3 - 2d^2\ln(3\tau)/3\tau + (3\tau)^{-1}\theta_0(k)\} \tag{20}$$

and

$$k^2 = -\chi/3\tau. \tag{21}$$

For large times (18) represents a rapid oscillation of the phase θ with a slow amplitude modulation $[\ln(1-|r(\frac{1}{2}k)|^2)]^{\frac{1}{2}}$ which depends on the initial data [through $r(\frac{1}{2}k)$]. Equation (21) can be interpreted as defining the group velocity for a wavenumber k, a concept from linear analysis which applies to this nonlinear problem as well. This surprising conclusion will be verified by the experiments.

Another interesting feature of the nonlinear solution is the relative decay rates of the wave front and trailing oscillations. From (18) the oscillations are seen to decay like $(3\tau)^{-\frac{1}{2}}$ while the wave front decays at the faster rate $[\ln(3\tau)/3\tau]^{-\frac{2}{3}}$. Hence, asymptotically, the trailing wave oscillations should become the most prominent feature of the wave train.

2.2. *The linear dispersive equation*

A simpler model equation can be obtained by linearizing (3) to yield

$$f_\tau + f_{\chi\chi\chi} = 0. \tag{22}$$

This linear equation has been used to model the propagation of long waves of small amplitude (see, for example, Jeffreys & Jeffreys 1972, pp. 512–517). The solution of (22) is

$$f(\chi,\tau) = \frac{1}{2\pi}\int_{-\infty}^{\infty} \mathscr{A}(k)\exp\left[i(k\chi + k^3\tau)\right]dk, \tag{23}$$

where $\mathscr{A}(k)$ is the Fourier transform of the initial data:

$$\mathscr{A}(k) = \int_{-\infty}^{\infty} f(\chi,0)\,e^{-ik\chi}d\chi. \tag{24}$$

The asymptotic approximation of (23) for large τ is easily found using the method of stationary phase and is conveniently described in terms of three regions. (Recall that four regions were required in the nonlinear analysis.) For $\chi = O(\tau)$, corresponding to region I in figure 1(*b*), the wave amplitude is found to be exponentially small just as in the nonlinear analysis. For the wave front, region II, where $|\chi| = O(\tau^{\frac{1}{3}})$, the linear analysis also predicts a similarity solution, which may be written in terms of the Airy function Ai as

$$f(\chi,\tau) = \frac{1}{(3\tau)^{\frac{1}{3}}}\left(\int_{-\infty}^{\infty} f(\chi,0)d\chi\right)\mathrm{Ai}\,(\zeta) + O[(3\tau)^{-1}]. \tag{25}$$

The shift in the co-ordinate system for the linear analysis is

$$\chi_0 = \int_{-\infty}^{\infty} \chi f(\chi, 0) d\chi \Big/ \int_{-\infty}^{\infty} f(\chi, 0) d\chi. \tag{26}$$

The amplitude of the wave front is seen from (25) to decay like $(3\tau)^{-\frac{1}{3}}$.

The asymptotic solution for the trailing wave structure in region IV, where $-\chi = O(\tau)$, is

$$f(\chi, \tau) = \frac{1}{\pi^{\frac{1}{2}}} \frac{\mathscr{A}(k)}{(3\tau k)^{\frac{1}{2}}} \cos\theta, \tag{27}$$

with

$$\theta = (3\tau)\{\tfrac{2}{3}k^3 + \tfrac{1}{4}\pi\}, \tag{28}$$

k being given by (21). Thus, according to linear analysis, the trailing waves are again found to be rapid oscillations of the phase θ modulated in amplitude, by $\mathscr{A}(k)/k^{\frac{1}{2}}$, which decay like $(3\tau)^{-\frac{1}{2}}$. Since the wave front is decaying more slowly (like $(3\tau)^{-\frac{1}{3}}$), asymptotically the wave front should become the most prominent feature of the wave train. This suggested behaviour is exactly opposite to that predicted by the nonlinear analysis and represents a feature of the solution which can be tested by the experiments.

For the rectangular initial wave given by (24), the Fourier transform and translation of the co-ordinate system become

$$\mathscr{A}(k) = -2(A/k) \sin \tfrac{1}{2}kL\, e^{\frac{1}{2}ikL}, \tag{29}$$

$$\chi_0 = \tfrac{1}{2}L. \tag{30}$$

The integral coefficient in (25), which represents the wave volume, becomes

$$\int_{-\infty}^{\infty} f(\chi, 0)\, d\chi = -AL. \tag{31}$$

In the companion paper (Hammack & Segur 1978) it has been shown that asymptotic linear dispersive theory is theoretically justifiable for the wave front (region II) only when both an Ursell number, based on the length and amplitude of the initial data, and the wave volume are small. Moreover, the linear and nonlinear solutions for the trailing wave region can be made formally to coincide only when an Ursell number based on the local wavelength k^{-1} and amplitude of the initial wave is small. In the experiments presented herein, these conditions are not satisfied, and the limitations of the asymptotic linear dispersive theory are demonstrated.

2.3. *The nonlinear Schrödinger equation*

The solutions of both the KdV equation and its linearized version indicate that modulated wave groups with high frequency (large k) carrier waves will evolve in the trailing wave region. The applicability of long-wave (small k) model equations for describing the evolution of these short waves is immediately suspect. Hasimoto & Ono (1972) as well as Yuen & Lake (1975) have shown that the proper model equation for describing the evolution of wave packets with short carrier waves is the nonlinear Schrödinger equation. Following Hasimoto & Ono (1972), a dimensional form of this equation in terms of a complex potential Q is

$$iQ_T + \mu Q_{XX} + \nu |Q|^2 Q = 0, \tag{32}$$

where T is a stretched (dimensional) time and $X = x - Vt$ with V equal to the group velocity of the carrier wave. The dimensional constants μ and ν are given by

$$2\mu = \omega_*''(k_*) = -(g/4k_*\sigma\omega_*)\{[\sigma - k_*h(1-\sigma^2)]^2 + 4k_*^2h^2\sigma^2(1-\sigma^2)\}, \tag{33a}$$

$$\nu = \frac{-k_*^4}{2\omega_*}\left\{\frac{1}{V^2-gh}\left[4\left(\frac{\omega_*}{k_*}\right)^2 + 4(1-\sigma^2)\frac{\omega_*}{k_*}V + gh(1-\sigma^2)^2\right] + \frac{1}{2\sigma^2}(9-10\sigma^2+9\sigma^4)\right\}, \tag{33b}$$

where $\sigma = \tanh k_*h$, ω_* and k_* are the dimensional frequency and wavenumber of the carrier waves, and $\omega_*(k_*)$ represents the linear dispersion relation. The dimensional wave amplitude η is

$$\eta = (i\omega_*/g)[Qe^{i\theta} - \text{c.c.}], \tag{34}$$

where $\theta = k_*x - \omega_*t$ and c.c. represents the complex conjugate.

It is well known that Stokes wave packets with carrier waves such that $k = k_*h > 1{\cdot}36$ are unstable (see Benjamin & Feir 1967; Whitham 1967; Benjamin 1967). Hasimoto & Ono (1972) point out that this information is obtainable from (32) since ν changes sign from negative to positive across $k = 1{\cdot}36$ as k decreases ($\mu < 0$ always). However, (32) remains a valid model equation even for the unstable wave.

The nonlinear Schrödinger equation was solved exactly using inverse scattering theory by Zakharov & Shabat (1972). It was shown that an initial pulse which decays in amplitude sufficiently rapidly as $|x| \to \infty$ evolves into a finite number of 'envelope solitons', each of whose amplitude, in an appropriate co-ordinate system, is given by

$$\eta_e(x,t) = a_0 \operatorname{sech}\left[\frac{a_0 g}{\omega_*}\left(\frac{\nu}{8\mu}\right)^{\frac{1}{2}}(x - Vt)\right], \tag{35}$$

where a_0 is the maximum envelope amplitude. These 'envelope solitons' are analogous to the long-wave solitons of the KdV equation and represent permanent wave forms which interact with each other without suffering any permanent change in shape.

In addition to the criterion ($k > 1{\cdot}36$) for envelope solitons to evolve, Ablowitz *et al.* (1974) also showed that in order to produce solitons the envelope of the initial pulse must satisfy

$$\bar{V}_e = \left(\frac{\nu}{\omega_*''}\right)^{\frac{1}{2}}\frac{g\omega_*'}{2\omega_*}\int_{-\infty}^{\infty}|\eta_e|\,dx > 0{\cdot}90, \tag{36}$$

where $\bar{V}_e$ is a dimensionless volume.

In summary, when a modulated wave group with a short carrier wave evolves from long initial waves, the subsequent behaviour of this group is expected to be modelled by the nonlinear Schrödinger equation (32). If the carrier waves are such that $k > 1{\cdot}36$ and the packet envelope satisfies (36), then envelope solitons similar to (35) may be anticipated.

The time required for envelope solitons to evolve from a modulated wave train is proportional to the length and inversely proportional to the amplitude of the modulation (Yuen & Lake 1975).

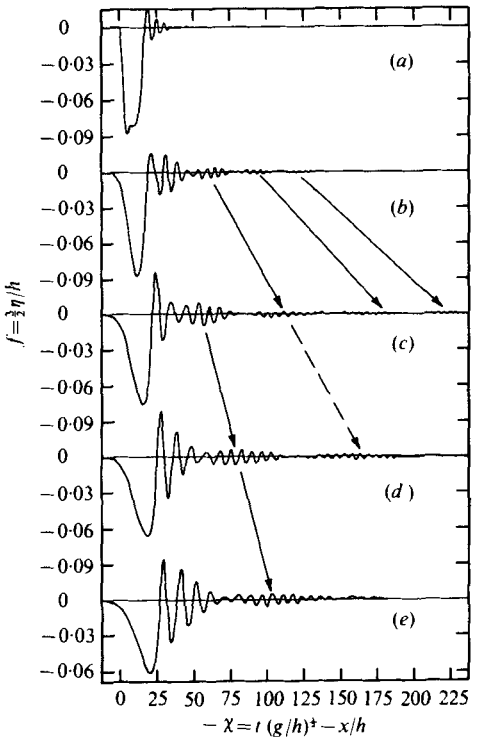

FIGURE 2. Experimental wave systems: $h = 10$ cm, $L_* = 122$ cm, $A_* = 0{\cdot}5$ cm, $M = 0{\cdot}0335$, $\chi_0 = -3{\cdot}66$. (*a*) $x/h = 0$ or $3\tau = 0$, (*b*) $x/h = 50$ or $3\tau = 25$, (*c*) $x/h = 100$ or $3\tau = 50$, (*d*) $x/h = 150$ or $3\tau = 75$, (*e*) $x/h = 200$ or $3\tau = 100$. →, trajectory based on average wavenumber between two stations and linear dispersion relation; – –→, extrapolation of previous trajectory.

3. Experiments

3.1. *Equipment and procedure*

The experimental equipment used in this study was described briefly in part 2 and in greater detail by Hammack (1973). The wave maker consists of a rectangular piston 61 cm long at the end of a wave tank. The rectangular wave propagating out of the generation region following a sudden downthrow of the piston has a length of twice the piston length and an amplitude of one-half the piston stroke. By varying the piston stroke while the quiescent water depth is fixed at $h = 10$ cm, the nonlinearity of the initial wave is varied. For all of the experiments presented herein the length of the initial wave is constant at $L_* = 122$ cm or $L = 12{\cdot}2$. The initial wave amplitudes are $A_* = 0{\cdot}5$ cm, $1{\cdot}5$ cm and $2{\cdot}5$ cm.

Waves are measured using parallel-wire resistance gauges and an oscillograph recorder at the following positions: $x = 0$, $50h$, $100h$, $150h$ and $200h$, where $x = 0$ is the downstream edge of the piston. Some of these measurements, especially those at $x = 200h$, are incomplete because the wave reflected from the downstream end of the tank returned prior to the complete passage of the rightward-running wave system. In the comparisons with theory, wave traces at $x/h = 0$, 50, 100, 150 and 200 are assumed to represent the spatial wave at the times $3\tau = 0$, 25, 50, 75 and 100, respectively, according to the normalization given by (2). Consequently, a rightward-

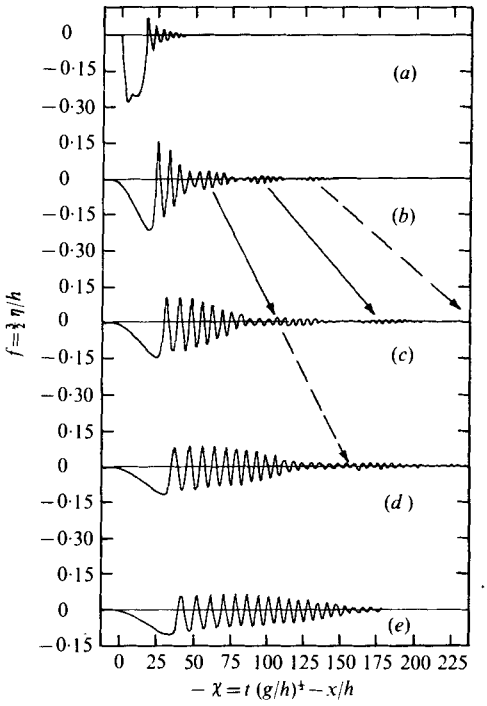

FIGURE 3. Experimental wave systems: $h = 10$ cm, $L_* = 122$ cm, $A_* = 1{\cdot}5$ cm, $M = 8{\cdot}36 \times 10^{-5}$, $\chi_0 = -2{\cdot}108$. (*a*) $x/h = 0$ or $3\tau = 0$, (*b*) $x/h = 50$ or $3\tau = 25$, (*c*) $x/h = 100$ or $3\tau = 50$, (*d*) $x/h = 150$ or $3\tau = 75$, (*e*) $x/h = 200$ or $3\tau = 100$. →, trajectory based on average wavenumber between two stations and linear dispersion relation; - →, extrapolation of previous trajectory.

running wave necessarily appears leftward-running, i.e. the wave front appears at the left in each figure. Moreover, a point moves to the left or right in succeeding measurements depending on whether its velocity is greater or less than $(gh)^{\frac{1}{2}}$, respectively.

In the comparison of theory and experiment for the trailing wave region, wavenumbers k are required; however, only wave frequencies $\omega = (h/g)^{\frac{1}{2}}\omega_*$ are directly measurable from the experiments. To compute wavenumbers from the measured frequencies, the complete (all k) dispersion relation for linear water waves

$$\omega^2 = k \tanh k \tag{37}$$

is used. This procedure is adopted since measured frequencies and the water depth $h = 10$ cm indicate that many of the oscillatory waves which evolve are not 'long' and considerable error is introduced by replacing (37) by its long-wave approximation.

3.2. *Observed wave evolution*

Figures 2–4 show the downstream wave measurements for three experiments with initial wave amplitudes of $A_* = 0{\cdot}5$ cm, $1{\cdot}5$ cm and $2{\cdot}5$ cm, respectively. The normalized wave amplitude f (or $\frac{3}{2}\eta/h$) is shown as a function of the non-dimensional co-ordinate $-\chi$ (or $t(g/h)^{\frac{1}{2}} - x/h$). Wave traces are presented in this manner to emphasize that they are in fact temporal measurements at a fixed spatial location. which are

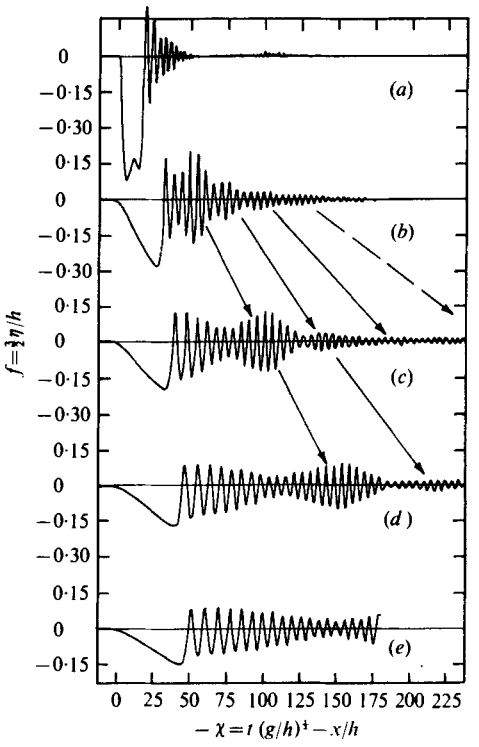

FIGURE 4. Experimental wave systems: $h = 10$ cm, $L_* = 122$ cm, $A_* = 2{\cdot}5$ cm, $M = 1{\cdot}73 \times 10^{-6}$, $\chi_0 = -1{\cdot}633$. (*a*) $x/h = 0$ or $3\tau = 0$, (*b*) $x/h = 50$ or $3\tau = 25$, (*c*) $x/h = 100$ or $3\tau = 50$, (*d*) $x/h = 150$ or $3\tau = 75$, (*e*) $x/h = 200$ or $3\tau = 100$. →, trajectory based on average wavenumber between two stations and linear dispersion relation; – –→, extrapolation of previous trajectory.

subject to an error $O(A)$ when interpreted as spatial records at a fixed time as required herein.

The initial wave measurement in all figures, corresponding to $3\tau = 0$ (or $x/h = 0$), consists primarily of a negative wave which is rectangular in shape. However, oscillatory waves have already formed during the time required for the wave to propagate past the wave gauge. In fact, the differences in the initial wave measurements in figures 2–4 from that shown in figure 1(*a*) represent the $O(A)$ error incurred in representing a spatial wave record by its temporal counterpart. These figures clearly show that the error is indeed enhanced as the amplitude of the initial data is increased.

During propagation, the initial wave quickly acquires a wave structure similar to that shown in figure 1 (*b*). The leading wave becomes 'triangular' in shape and propagates with a speed of approximately $(gh)^{\frac{1}{2}}$. The amplitude of the leading wave decreases during propagation through the combined action of frequency separation and viscosity while the slope of its frontal face also decreases. Modulated wave groups emerge in the trailing wave region of the wave train and disperse behind the leading wave, indicating group velocities which are less than $(gh)^{\frac{1}{2}}$.

It should be emphasized that the wave evolution observed in figures 2–4 is from initial data which are identical except for amplitude. If the subsequent propagation of each initial wave were linear, equivalent downstream measurements in each figure would be identical except for a proportionality factor in amplitude. It is evident from

these figures that nonlinearity is affecting wave evolution. For example, the amplitudes of the oscillatory waves increase relative to that of the leading wave as the nonlinearity is increased. This behaviour is similar to that suggested by the nonlinear analysis of § 2.1, where the decay rate for the leading wave was found to be faster than that for the oscillatory waves. (Opposite behaviour is suggested by the linear analysis in § 2.2.) Nonlinearity also appears to increase carrier wave frequencies of corresponding wave groups. A more quantitative comparison of carrier wavenumbers will be presented in § 4.2.1.

An interesting phenomenon occurs in figure 3 during the propagation between the third and fourth measurement stations. At the third station two well-formed wave groups (node-to-node) are observed to be following the dispersive waves behind the shock region. However, at the fourth station the leading group appears to have disintegrated, forming an irregular wave train with little apparent order. Examination of this wave group at the third station indicates a carrier wave frequency of $\omega = 1{\cdot}17$, which corresponds to a wavenumber $k = 1{\cdot}50$ according to the dispersion relation (37). Hence the wave packet is unstable ($k > 1{\cdot}36$) and the subsequent disintegration of this group is apparently a manifestation of the wave instability discussed in § 2.3. For this particular experiment, no envelope soliton evolves in the test section of the wave tank.

4. Comparison of theory and experiment

4.1. *Leading wave*

For the wave front we limit our attention to the profile and maximum amplitude of the leading wave in region II of figure 1 (*b*). Both the linear and the nonlinear analysis of § 2 describe the wave in this region in terms of a similarity solution with a space-like variable $\zeta = (\chi+\chi_0)/(3\tau)^{\frac{1}{3}}$. The nonlinear asymptotic solution is given by (10) while the linear asymptotic solution is given by (25). Numerical values for the co-ordinate shift χ_0 and the parameter M required in the nonlinear solution are indicated in the figure captions for each experiment. [These parameters are computed from (14).] The co-ordinate shift for the linear analysis, given by (30), depends only on the length of the initial data; hence $\chi_0 = 6{\cdot}1$ for every experiment.

Theoretical profiles for the wave front corresponding to the last measured wave trace in figure 4 ($3\tau = 100$ or $x/h = 200$) are shown in figure 5, superimposed on the experimental record. This comparison of the linear theory, the KdV theory and the experiment is so striking that perhaps no additional comment is necessary! The discrepancy between the KdV solution and the measured location of the amplitude extremum is probably due to viscous effects in the measured data. Viscosity, whose effects are not modelled by either asymptotic solution, is expected to attenuate wave amplitudes through viscous energy dissipation and to 'stretch' the leading wave since boundary shear forces will reduce the wave speed near the amplitude extremum below that in region I of the wave front, where amplitudes are exponentially small. This stretching effect is illustrated in figure 5 by a wave trace taken from Lee & Kim (1978) representing a solution of a KdV-type equation modified to include the effects of boundary shear. Their solution, which is computed numerically using the initial wave in figure 4 as the initial data, predicts well the location of the amplitude extremum.

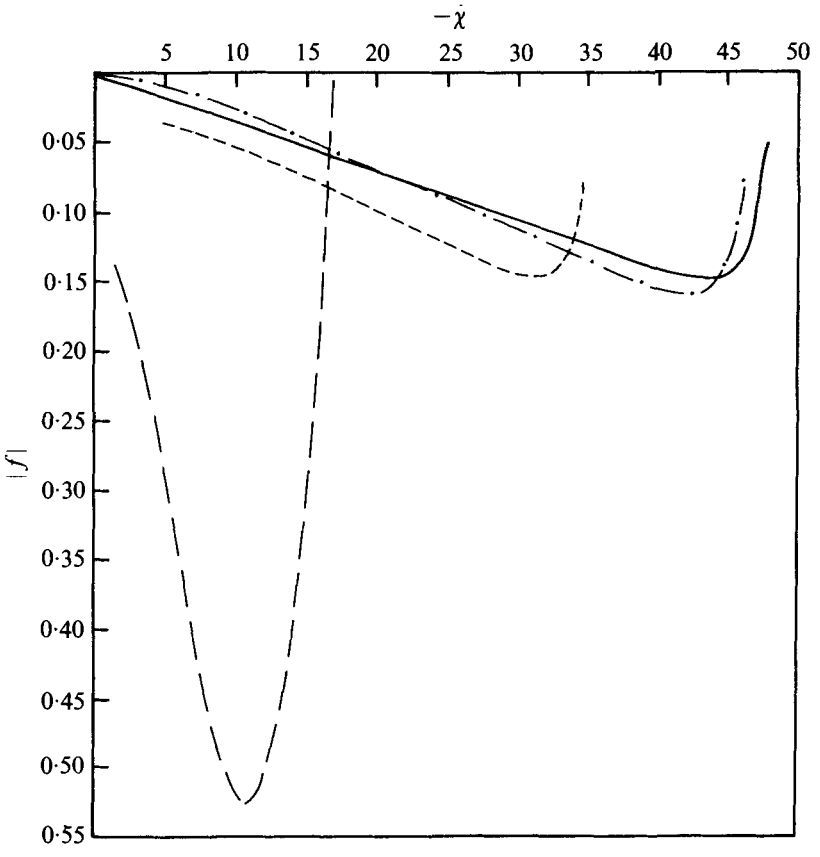

FIGURE 5. Theoretical and experimental profiles for wave front corresponding to $3\tau = 100$ in experiment shown in figure 4. ——, experiment; – –, linear asymptotic theory; ····, KdV asymptotic theory; –·–, numerical solution of a viscous–KdV theory, after Lee & Kim (1978).

The agreement between the maximum amplitude predicted by the KdV equation and the measured data is not always as good as that shown in figure 5. Figure 6 shows a comparison of measured and predicted wave amplitudes as a function of time 3τ (or x/h); results are shown separately for each experiment. The linear solutions shown in figure 6 represent a decay rate for the leading wave of $(3\tau)^{-\frac{1}{2}}$ while the nonlinear solution, for large times, represents the faster decay rate of $[\ln(3\tau)/3\tau]^{\frac{1}{2}}$. The divergence of these theoretical results for large times is clearly evident in figure 6. For the experiment with weakest nonlinearity (figures 2 and 6*a*), the measured amplitudes are smaller than those predicted by either theoretical solution. However, as time increases, the measured data approach the KdV solution. This behaviour is more apparent for the experiments with larger amplitudes, shown in figures 6(*b*) and (*c*). Clearly, over the range of times considered, the inviscid KdV solution provides a better estimate of measured amplitudes than the inviscid linear solution.

In summary, over the range of initial data and propagation times investigated, linear asymptotics, as expected, fail to predict accurately any quantitative details of the leading wave. The KdV asymptotic solution provides a more accurate descrip-

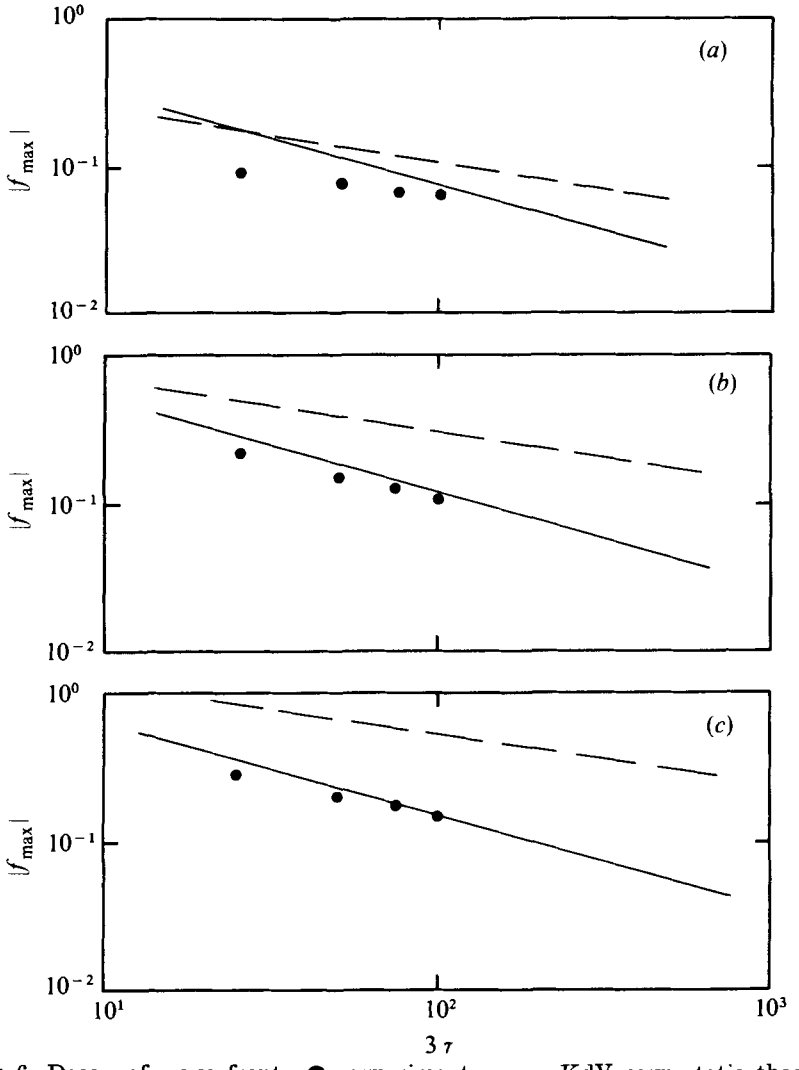

FIGURE 6. Decay of wave front: ●, experiment; ——, KdV asymptotic theory; – –, linear asymptotic theory. (*a*) Experiment in figure 2. (*b*) Experiment in figure 3. (*c*) Experiment in figure 4.

tion of observed wave behaviour; discrepancies that still exist appear to be due to viscous effects in the experiments.

4.2. *Trailing wave oscillations*

The outstanding features of the oscillatory waves in region IV (see figure 1*b*), as predicted by either the nonlinear or the linear theory, are as follows.

(i) The initial data produce definite node-to-node wave groups, each dominated by a single wavenumber.

(ii) Each wave group propagates with a speed equivalent to the linear group velocity of its dominant wavenumber.

(iii) The amplitude of each wave group is determined by the initial data.

(iv) Long initial waves will produce some wave groups with short carrier waves. If the dominant wavenumber of these groups satisfies $k > 1{\cdot}36$, instabilities may occur which evolve according to the nonlinear Schrödinger equation.

In this section each of these predicted features of the trailing wave oscillations is compared with the observed behaviour in the water-wave experiments shown in figures 2–4.

4.2.1. *Wavenumbers.* The nonlinear solution (22) for the oscillatory wave region predicts a slow amplitude modulation given by $[\ln(1-|r(\frac{1}{2}k)|^2)]^{\frac{1}{2}}$; hence nodes are located at the zeros of the reflexion coefficient $r(\frac{1}{2}k)$. For rectangular initial waves, $r(\frac{1}{2}k)$, given by (7), has nodes at

$$(\tfrac{1}{4}k^2 - A)^{\frac{1}{2}} L = p\pi, \quad p = 0, 1, 2, \ldots . \tag{38}$$

It is convenient to assume the dominant wavenumber in a group to be the value at the midpoint between adjacent nodes, or

$$(\tfrac{1}{4}k_m^2 - A)^{\frac{1}{2}} L = \tfrac{1}{2}(2m-1)\pi, \quad m = 1, 2, \ldots , \tag{39}$$

which yields

$$k_m(\mathrm{KdV}) = \{4A + (2m-1)^2\pi^2/L^2\}^{\frac{1}{2}}, \quad m = 1, 2, \ldots . \tag{40}$$

The role of the initial amplitude A in determining group wavenumbers is clearly demonstrated by (40); nonlinearity increases the dominant wavenumber.

For the linear solution, given by (27), the nodes of the groups occur at the zeros of $\mathscr{A}(k)$, or at

$$\tfrac{1}{2}kL = p\pi, \quad p = 1, 2, \ldots . \tag{41}$$

Midway between nodes, the dominant wavenumbers are given by

$$k_n(\mathrm{linear}) = (2n+1)\pi/L, \quad n = 1, 2, \ldots . \tag{42}$$

According to both the linear and the nonlinear analysis, wave groups which evolve should disperse according to the linear group velocity of their carrier waves. Hence the groups should order themselves with k increasing towards the rear of the wave train.

By comparing (18), (7), (27) and (29), it can be shown that the linear and nonlinear solutions for the trailing waves are equivalent when

$$Ak^{-2} \ll 4. \tag{43}$$

The parameter Ak^{-2} is a local Ursell number based on the amplitude of the initial data and the local wavelength. The condition (43) is satisfied by the carrier waves for groups corresponding to large m or n; hence, if we require $k_m(\mathrm{KdV}) = k_n(\mathrm{linear})$ for large m and n then m and n must be related by $n = m-1$. Finally the dominant wavenumbers according to the linear solution may be written in terms of m as

$$k_m(\mathrm{linear}) = (2m-1)\pi/L, \quad m = 2, 3, \ldots . \tag{44}$$

Comparison of allowable values for m in (40) and (44) suggests that there exists an 'extra' node-to-node wave group immediately behind the shock region (corresponding to $m = 1$) for the nonlinear solution which has no linear counterpart. The dominant wavenumber k_1 of this extra wave group is always smaller than the first dominant wavenumber predicted by linear analysis.

In order to compare wavenumbers predicted by asymptotic (large-time) solutions

Wave group (m)	Linear		KdV		Measured k			
	k_m	$3\tau_s$	k_m	$3\tau_s$	$3\tau = 25$	$3\tau = 50$	$3\tau = 75$	$3\tau = 100$
				(a)				
1	—	—	0·61	39	—	'0·64'	'0·65'	'0·65'
2	0·77	27	0·95	20	'0·75'	1·00	1·02	1·02
3	1·29	14	1·40	13	1·45	1·60	1·55	—
4	1·80	11	1·88	10	2·00	1·90	—	—
5	2·32	9	2·38	9	2·40	2·40	—	—
				(b)				
1	—	—	0·98	19	—	—	—	—
2	0·77	27	1·22	15	'1·01'	'1·12'	'1·10'	'1·12'
3	1·29	14	1·60	12	1·50	1·50	—	—
4	1·80	11	2·04	10	2·10	2·20	—	—
5	2·32	9	2·50	9	2·80	—	—	—
				(c)				
1	—	—	1·25	15	'1·10'	'0·95'	'0·95'	'0·95'
2	0·77	27	1·45	13	1·50	1·60	1·50	—
3	1·29	14	1·78	11	1·72	1·85	1·90	—
4	1·80	11	2·18	10	2·05	2·20	—	—
5	2·32	9	2·62	9	2·50	2·45	—	—

TABLE 1. Theoretical and experiment wavenumbers for trailing wave groups: (a) experiment in figure 2, (b) experiment in figure 3, (c) experiment in figure 4. Numbers in inverted commas represent the average wavenumber in oscillations preceding the first node-to-node wave group.

with finite-time experiments, it is important to determine the time scale required for asymptotic conditions to evolve. This can be done crudely by adopting the following point of view, based on assumed linear behaviour. The leading wave ($k = 0$) propagates with a speed $(gh)^{\frac{1}{2}}$ while wave groups propagate with the linear group velocity V of their carrier waves. Hence the wave front and a specific wave group move relative to each other with a speed $S = (gh)^{\frac{1}{2}} - V$. A wave group should evolve in the time t_s required for the wave front and group to move, relative to each other, the length of the initial data. Hence an approximate magnitude of the sorting time for a wave group is

$$t_s = L_*/S \quad \text{or} \quad 3\tau_s = \tfrac{1}{2}t_s(g/h)^{\frac{1}{2}}. \tag{45}$$

It should be emphasized that (45) is based on the assumption of linear behaviour for all waves (all k) during their initial interaction. Nonlinear analysis does indicate that waves propagate with linear speeds once separated; however, it is not clear (or expected) that this is valid during initial propagation. Experiments will show that nonlinear effects appear to increase significantly the sorting time over that predicted by (45) for groups with small k.

Theoretical and measured wavenumbers are shown in tables 1 (a), (b) and (c) for the experiments presented in figures 2, 3 and 4, respectively. Experimental wavenumbers are computed from measured frequencies using the dispersion relation (37); results for all observable groups are shown at each time 3τ (or x/h) of measurement. In addition, an average wavenumber is shown in inverted commas for the oscillatory waves between the shock region and the node of the leading group. Prior to the

evolution of asymptotic conditions, the average wavenumber in this region should be representative of the next node-to-node group to emerge. The predictions of k by linear analysis are the same for each experiment; there is no linear prediction for $m = 1$. Sorting times $3\tau_s$ are listed for each k predicted by the linear or nonlinear analysis.

In order to align the k measured at a finite time with the theoretical (and asymptotic) results, observable wave groups at $3\tau = 25$ are 'fitted' to the theoretical k with sorting times which satisfy $3\tau_s < 25$. Once the measured data are aligned at $3\tau = 25$, results at subsequent times are automatically located, since the dominant wavenumbers of all asymptotic groups should remain constant and each group should propagate with the group velocity of its carrier wave. This procedure is demonstrated best by the results in table 1 (*a*), for the experiment (figure 2) with weakest nonlinearity. At $3\tau = 25$ three groups are observed. These groups align best with the theoretical computations corresponding to $m = 3$, 4 and 5, which have sorting times significantly smaller than the time of measurement. Note that for all three groups the nonlinear prediction of k agrees with the observed results better than does the linear prediction. Between the shock region and the partial node of the leading wave group, the average wavenumber is 0·75. At the next station of measurement, $3\tau = 50$, wavenumbers for the groups corresponding to those at $3\tau = 25$ have remained relatively constant. A new group has emerged at $3\tau = 50$ with $k = 1{\cdot}00$; this agrees well with the nonlinear prediction (but not the linear prediction) corresponding to $m = 2$. The average wavenumber of the oscillations preceding this wave group has now decreased to 0·64, which is approximately equal to the nonlinear prediction $k = 0{\cdot}61$ for $m = 1$. At the subsequent times of measurement, the number of observable wave groups is reduced owing to the return of the reflected wave from the end of the channel and attenuation by viscosity. Wavenumbers for the observable groups remain constant during propagation; however, a node-to-node wave group with $k = 0{\cdot}61$, corresponding to $m = 1$, does not emerge even though its suggested sorting time ($3\tau_s = 39$) is exceeded by the measurement times. The average wavenumber in the oscillations preceding the first group remains constant with a value of approximately 0·65. This behaviour suggests that the wave group corresponding to $m = 1$ (with no linear counterpart) is present but requires much longer to evolve than the 'linear' sorting time given by (45). Wave groups with $k > 1{\cdot}36$ do not disintegrate during the time of measurement in this experiment.

The measured data in table 1 (*b*), corresponding to the experiment in figure 3, are more difficult to align than those in table 1 (*a*). At $3\tau = 25$ three groups are observable which appear to represent asymptotic groups corresponding to $m = 3$, 4 and 5. Again the measured results agree better with the nonlinear prediction although not as consistently as the data in table 1 (*a*). Measured data at subsequent times are again limited by reflexion and attenuation. In addition, the leading wave group at $3\tau = 25$, which has a dominant wavenumber $k > 1{\cdot}36$, disintegrates before $3\tau = 75$, and a dominant wavenumber is no longer measurable. No additional wave groups emerge after $3\tau = 25$ even though two groups, corresponding to $m = 1$ and 2, have sorting times which are exceeded by the measurement times. The average wavenumber between the shock region and node of the leading group remains relatively constant at a value between the nonlinear predictions for k_1 and k_2. This behaviour suggests that nonlinearity might be affecting the sorting time of the first two groups in this experiment.

The measured data in table 1(*c*), corresponding to the experiment (figure 4) with the biggest waves, align well with the nonlinear predictions for $k_2, \ldots, k_5$. The inapplicability of the linear solution for small m is apparent in this experiment. Again the measured k for each group remains approximately constant as the group propagates. The wave group corresponding to $m = 1$ does not evolve during the time of measurement while the average wavenumber between the shock and node of the leading group remains constant at a value below the predicted k_1. Notice that for $m \geqslant 2$ both the k predicted by the nonlinear analysis and all measured k are in the unstable range $k > 1{\cdot}36$. Although no disintegration is observed, it will be shown in §§4.2.3 and 4.2.4 that at least one observable group in figure 4 is actually an envelope soliton. In other words, the initial wave in figure 4 appears to evolve deep-water solitons prior to the first time of measurement. The carrier wavenumber of each envelope soliton appears to be predicted well by the long-wave analysis based on the KdV equation.

4.2.2. *Group velocities.* The nonlinear analysis of §2.1 indicates that a wave group should propagate with the linear group velocity associated with its carrier wave. Theoretical trajectories of observable wave groups are shown superposed on the wave records in figures 2–4. These trajectories are found by computing the linear group velocity based on the average wavenumber of a group between two stations of measurement (see tables 1*a–c*). Trajectories shown dashed represent an extension of the trajectory between the two previous stations. In all cases, actual group positions agree well with those predicted by linear dispersion, even when the groups still overlap at their extremities as in figure 4.

4.2.3. *Envelope amplitudes.* In this subsection we compare measured and predicted values of envelope amplitudes for the asymptotic wave groups. Unlike wavenumbers and group velocities, the measured amplitudes are expected to be significantly affected (attenuated) by viscosity. No effort will be made herein to model these effects; hence comparison of measured amplitudes with theoretical predictions based on inviscid theories is necessarily limited to qualitative features.

To leading order, the envelope amplitude according to the nonlinear analysis of §2.1 is found from (18) and (19) to be

$$(k/3\tau)^{\frac{1}{2}}\{-\pi^{-1}\ln[1-|r(\tfrac{1}{2}k)|^2]\}^{\frac{1}{2}}. \tag{46}$$

If it is assumed that the maximum amplitude f_e of the envelope occurs midway between nodes, then using (40), (46) and (7) gives

$$f_e(\mathrm{KdV}) = \left(\frac{k_m}{3\tau\pi}\right)^{\frac{1}{2}}\left\{-\ln\left[1-\left(\frac{2A}{k_m^2-2A}\right)^2\right]\right\}^{\frac{1}{2}}. \tag{47}$$

In a similar manner, the corresponding maximum envelope amplitude according to the linear analysis of §2.2 is found to be

$$f_e(\mathrm{linear}) = \left(\frac{k_m}{3\tau\pi}\right)^{\frac{1}{2}}\frac{2A}{k_m^2}. \tag{48}$$

Notice that the nonlinear and linear predictions for f_e are equivalent when m (or k_m) is large. In addition, nonlinear effects cause a reduction in the predicted amplitude for small m.

Group (m)	KdV k	$3\tau = 25$ Meas.	Linear	KdV	$3\tau = 50$ Meas.	Linear	KdV	$3\tau = 75$ Meas.	Linear	KdV	$3\tau = 100$ Meas.	Linear	KdV
						(a)							
2	0·95	—	—	—	108	176	158	71	144	129	62	125	111
3	1·40	68	116	111	30	82	75	25	67	64	—	—	—
4	1·88	30	70	68	14	49	48	—	—	—	—	—	—
5	2·38	15	48	47	—	—	—	—	—	—	—	—	—
						(b)							
3	1·60	430	347	308	230	246	218	—	—	—	—	—	—
4	2·04	230	210	197	150	148	139	—	—	—	—	—	—
5	2·50	150	144	138	—	—	—	—	—	—	—	—	—
						(c)							
2	1·45	1990	1245	827	1370	881	585	104	719	478	—	—	—
3	1·78	830	579	481	410	409	340	300	334	277	—	—	—
4	2·18	420	350	315	190	247	223	—	—	—	—	—	—
5	2·62	240	240	225	—	—	—	—	—	—	—	—	—

TABLE 2. Theoretical and experimental envelope amplitudes ($f_e \times 10^4$) of trailing wave groups: (a) experiment in figure 2, (b) experiment in figure 3, (c) experiment in figure 4.

Measured and predicted amplitudes f_e are shown in tables 2(a), (b) and (c) for the observable wave groups in figures 2, 3 and 4, respectively. Group identification is identical to that shown in tables 1(a), (b) and (c); nonlinear predictions for the wavenumber are also shown. The measured amplitudes in table 2(a) for the experiment with weakest nonlinearity are approximately one-half the predicted amplitudes. This behaviour is expected and at least part of the discrepancy can be attributed to viscous attenuation. A more definitive statement cannot be made since the dimensional amplitudes of the groups in table 2(a) are less than 1 mm, which is approaching the resolution limitations of the gauge used in measurements. Repetition of measurements for the initial amplitudes of the groups with $m = 2$ and 3 in table 2(a) indicated a scatter of $\pm 25\%$. Hence not all of the discrepancy between the experimental and theoretical results for these groups can be attributed to measurement errors. Viscosity does appear to be contributing to differences between measured and predicted results.

The measured envelope amplitudes in tables 2(b) and (c) exhibit a surprising behaviour: most of the measurements exceed the theoretical predictions. This behaviour is especially apparent for the leading group in table 2(c) at $3\tau = 25$, whose measured amplitude is 240% greater than that predicted by nonlinear analysis. (Recall that the data in table 2(c) correspond to the experiment in figure 4, where the nonlinearity is largest.) This behaviour is opposite to that expected and observed in table 2(a) and strongly suggests that the long-wave model equations are no longer applicable for these wave groups. The wave instability observed in figure 3 has already indicated the same conclusion; however, no disintegration is observed in figure 4. Since the observed groups in figure 4 appear to be stable even though their amplitudes are not modelled by the long-wave equations considered herein, it is possible that these groups are envelope solitons. This hypothesis will be tested in the next subsection.

4.2.4. *Evolution of envelope solitons.* Wave groups with carrier waves in the unstable

Experiment	3τ	Group (m)	Measured k	$\bar{V}_e$
Figure 2	25	3	1·45	0·07
		4	2·00	0·06
		5	2·40	$\ll 0{\cdot}06$
Figure 3	25	4	2·10	0·77
		5	2·80	0·57
	50	3	1·50	0·44
Figure 4	50	2	1·60	3·64
		3	1·85	2·06
		4	2·20	—
		5	2·45	—

TABLE 3. Non-dimensional volume of unstable wave groups observed in experiments.

regime, $k > 1{\cdot}36$, evolve in each experiment presented. The asymptotic behaviour of each of these groups is modelled by the nonlinear Schrödinger equation. Consequently, an unstable group should evolve a finite number of envelope solitons whose shape is given by (35). The number of solitons is zero unless the volume V_e of the wave packet is large enough to satisfy (36).

Table 3 shows the non-dimensional volume $\bar{V}_e$ of each wave group with $k > 1{\cdot}36$ in the experiments presented in § 3.2. Computations of $\bar{V}_e$ are made at the first station at which the group is sufficiently separated from surrounding waves. (Wave groups corresponding to $m = 4$ and 5 for the experiment shown in figure 4 do not separate sufficiently during observation for volumes to be computed.) The unstable groups in figure 2 have exceedingly small volumes; hence no deep-water solitons should evolve from either of these groups. In addition, group amplitudes are very small; this indicates that a large time is required before asymptotic conditions predicted by the nonlinear Schrödinger equation evolve. Since the time of observation is limited, it is not surprising that the wave groups retain their identity during this time and appear to be described by long-wave model equations.

None of the unstable groups in figure 3 has sufficient volume to produce deep-water solitons. However, the leading group at $3\tau = 50$ ($m = 3$) does disintegrate during subsequent observation; this behaviour is apparently a manifestation of the asymptotic condition when no solitons are present. A smaller time for asymptotic conditions to occur than in figure 2 is expected since group amplitudes have been increased in this experiment. (Corresponding group lengths are approximately equal in figures 2–4.)

The two leading groups at $3\tau = 50$ in figure 4 are seen from table 3 to have sufficient volume for each to produce at least one deep-water soliton. In addition, the time expected for these solitons to evolve should be small relative to that in figure 3 since group amplitudes have increased significantly. In fact, the leading group already appears to have evolved into a soliton shape by $3\tau = 50$. This behaviour is demonstrated in figure 7, where soliton shapes based on (42) and measured group amplitudes are shown superposed on the wave traces at $3\tau = 50$ and 75. In both cases, the frontal portion of the group agrees well with the soliton shape while the leeward portion is both steeper and smaller in amplitude than that of the soliton profile. This asymmetry apparently is not predicted by the theory, although it seems to be a typical

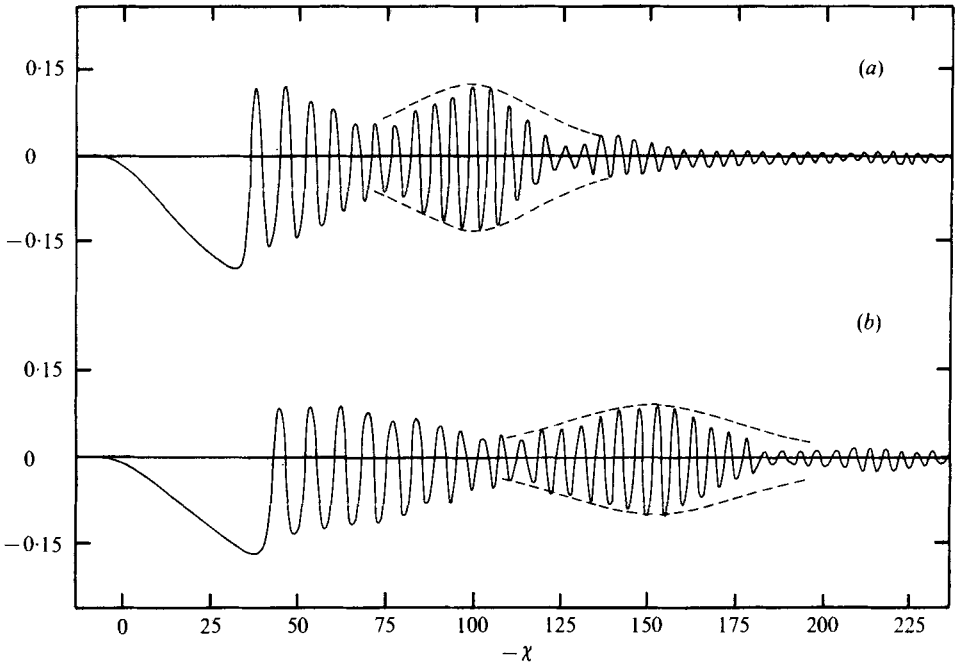

FIGURE 7. Evolution of envelope solitons for experiment shown in figure 4: ——, experiment; – –, theoretical profile of envelope soliton. (*a*) $x/h = 100$ or $3\tau = 50$, (*b*) $x/h = 150$ or $3\tau = 75$.

feature of deep-water solitons measured in a laboratory. It appears not only in these experiments, but also in the data of Yuen & Lake (1975) and of Feir (1967). It may be caused by viscous effects.

From these results, it appears that the KdV and nonlinear Schrödinger equation can be patched together to describe completely the evolution of two-dimensional water waves. If the initial wave is short ($k > 1{\cdot}36$), then linear dispersive theory followed by the nonlinear Schrödinger equation should describe the complete wave evolution. If the initial wave is long, then the KdV equation can be used to determine the dominant wavenumber and amplitude (or energy) of each unstable wave group. Subsequent evolution of each of these groups is modelled by the nonlinear Schrödinger equation.

5. Conclusions

The following conclusions may be stated on the basis of the water-wave experiments presented herein and their comparison with the KdV and linear long-wave models.

(i) An initially long negative wave produces no solitons. Instead, a wave train similar to that shown in figure 1(*b*) is produced, i.e. a negative triangular wave, travelling with a speed $(gh)^{\frac{1}{2}}$, followed by a train of modulated oscillatory waves which travel more slowly.

(ii) The amplitude of the leading wave decreases with time. Over the parameter range of the experiments, amplitudes predicted by asymptotic KdV theory are in error by no more than 20 % at the largest time of observation ($3\tau = 100$) whereas errors

in the linear asymptotic predictions always exceed 70%. The KdV predictions improve as the amplitude of the initial data is increased while the linear predictions become less credible.

(iii) The observed decay rate of the leading wave exceeds that of the trailing oscillations; hence the leading wave becomes less prominent with time. This behaviour is predicted by the KdV model, whereas the linear model predicts the opposite.

(iv) The trailing oscillations appear in definite groups, or wave packets. Once a wave packet has emerged, its dominant wavenumber remains approximately constant. The group propagates with the linear group velocity of its dominant wave.

(v) The time required for a particular wave group, characterized by its dominant wavenumber, to emerge increases with increasing amplitude and decreases with increasing wavenumber.

(vi) The dominant wavenumbers predicted by the KdV model agree with those observed in groups which emerge in the experiments to within approximately 10%. The dominant wavenumbers predicted by the linear theory agree with observations only when they also agree with the KdV model.

(vii) The KdV model predicts the existence of one node-to-node wave group with a dominant wavenumber smaller than the first predicted by linear analysis. This wave group does not emerge in the observation times of the experiments; however, there is some evidence that this group does exist.

(viii) Even though the initial wave is long, waves in these packets can be short, i.e. $k > 1{\cdot}36$. During subsequent propagation, these wave packets may disintegrate or focus into an envelope soliton. Neither possibility is predicted by the KdV or any other long-wave model. There is some evidence that the KdV equation and the nonlinear Schrödinger equation can be patched together to predict the complete evolution of these groups.

(ix) The amplitudes of the wave groups predicted by either the KdV or the linear model can differ from the observed amplitudes by 100% or more. Both viscosity and short-wave evolution appear to play a role in determining these amplitudes.

One author (J.H.) is indebted to the Mathematics Department, Clarkson College, for providing summer support which made this paper possible. He would also like to acknowledge his colleague (H.S.), who provided the major inspiration for the work presented herein. This work was supported by NSF Grants DES 75-06537 and MCS 75-07568A02 at the Department of Mathematics, Clarkson College and the Engineering Industrial Experiment Station at the University of Florida. Experiments were performed at the W. M. Keck Laboratory of Hydraulics and Water Resources, California Institute of Technology.

REFERENCES

ABLOWITZ, M. J., KAUP, D. J., NEWELL, A. C. & SEGUR, H. 1974 The inverse scattering transform – Fourier analysis for nonlinear problems. *Stud. Appl. Math.* **53**, 249–315.

ABLOWITZ, M. J. & SEGUR, H. 1977 Asymptotic solutions of the Korteweg–de Vries equation. *Stud. Appl. Math.* (to appear).

BENJAMIN, T. B. 1967 Instability of periodic wave trains in nonlinear dispersive systems. *Proc. Roy. Soc.* A **299**, 59–75.

BENJAMIN, T. B. & FEIR, J. E. 1967 The disintegration of wave trains on deep water. *J. Fluid Mech.* **27**, 417–430.

FEIR, J. E. 1967 Discussion: some results from wave pulse experiments. *Proc. Roy. Soc.* A **299**, 54–58.

HAMMACK, J. L. 1973 A note on tsunamis: their generation and propagation in an ocean of uniform depth. *J. Fluid Mech.* **60**, 769–799.

HAMMACK, J. L. & SEGUR, H. 1974 The Korteweg–de Vries equations and water waves. Part 2. Comparison with experiments. *J. Fluid Mech.* **65**, 289–314.

HAMMACK, J. L. & SEGUR, H. 1978 Modelling criteria for long water waves. *J. Fluid Mech.* **84**, 359–373.

HASIMOTO, H. & ONO, H. 1972 Nonlinear modulation of gravity waves. *J. Phys. Soc. Japan* **33**, 805–811.

JEFFREYS, H. & JEFFREYS, B. S. 1972 *Methods of Mathematical Physics*, 3rd edn. Cambridge University Press.

LEE, J.-J. & KIM, S. T. 1978 A viscous model for the propagation of nonlinear dispersive long waves. Submitted to *J. Fluid Mech.*

SCHIFF, L. I. 1968 *Quantum Mechanics*, 3rd edn. McGraw-Hill.

SEGUR, H. 1973 The Korteweg–de Vries equation and water waves. Part 1. Solution of the equation. *J. Fluid Mech.* **59**, 721–736.

WHITHAM, G. B. 1967 Nonlinear dispersion of water waves. *J. Fluid Mech.* **27**, 399–412.

YUEN, H. C. & LAKE, B. M. 1975 Nonlinear deep-water waves: theory and experiment. *Phys. Fluids* **18**, 956–960.

ZAKHAROV, V. E. & SHABAT, A. B. 1972 Exact theory of two-dimensional self focusing and one-dimensional self modulation of waves in nonlinear media. *Sov. Phys., J. Exp. Theor. Phys.* **34**, 62–69.